Resonant Auger Scattering by Attosecond X-Ray Pulses

Quan-Wei Nan(南全伟)[1†], Chao Wang(王超)[1†], Xin-Yue Yu(余心悦)[1†], Xi Zhao(赵曦)[1], Yongjun Cheng(程勇军)[1], Maomao Gong(宫毛毛)[1], Xiao-Jing Liu(刘小井)[2], Victor Kimberg[3], and Song-Bin Zhang(张松斌)[1*]

[1]*School of Physics and Information Technology, Shaanxi Normal University, Xi'an 710119, China*
[2]*School Physical Science and Technology, ShanghaiTech University, Shanghai 201210, China*
[3]*International Research Center of Spectroscopy and Quantum Chemistry–IRC SQC, Siberian Federal University, Krasnoyarsk 660041, Russia*

(Received 7 July 2023; accepted manuscript online 31 July 2023)

As x-ray probe pulses approach the subfemtosecond range, conventional x-ray photoelectron spectroscopy (XPS) is expected to experience a reduction in spectral resolution due to the effects of the pulse broadening. However, in the case of resonant x-ray photoemission, also known as resonant Auger scattering (RAS), the spectroscopic technique maintains spectral resolution when an x-ray pulse is precisely tuned to a core-excited state. We present theoretical simulations of XPS and RAS spectra on a showcased CO molecule using ultrashort x-ray pulses, revealing significantly enhanced resolution in the RAS spectra compared to XPS, even in the subfemtosecond regime. These findings provide a novel perspective on potential utilization of attosecond x-ray pulses, capitalizing on the well-established advantages of detecting electron signals for tracking electronic and molecular dynamics.

DOI: 10.1088/0256-307X/40/9/093201

X-ray photoelectron spectroscopy (XPS) is a widely used essential experimental technique in various fields including atomic and molecular physics, chemical science, and surface science.[1–3] Recent advancements in ultrashort x-ray and UV pulse sources, such as high harmonic generation[4,5] and x-ray free electron laser sources (XFELs),[6–8] have enabled the development of time-resolved x-ray photoelectron spectroscopy (TXPS).[9–11] TXPS serves as a complementary approach to the well established time-resolved photoelectron spectroscopy (TRPS) utilizing sub-picosecond ultraviolet pulses. Noticeably, TRPS can balance both high temporal and spectral resolutions to discern coupled electronic and nuclear dynamics[12–14] as well as chemical reactions.[15,16]

The utilization of x-ray pulses in sub-femtosecond and attosecond regime[17–21] has proven to be successful in investigating ultrafast femtosecond and attosecond vibronic dynamics within the framework of transient absorption spectroscopy.[22,23] However, when applied to XPS with ultrashort x-ray pulses, the broad bandwidth of subfemtosecond and attosecond pulses results in the smearing of intricate spectral structures associated with vibrational dynamics. Consequently, the applicability of photoelectron spectroscopy is significantly limited.[24,25] It is worth noting that when combined with an infrared (IR) pump pulse, attosecond photoelectron spectroscopy has been developed into new techniques, such as attosecond streak cameras and RABBITT (reconstruction of attosecond beating by interference of two-photon transitions), allowing for imaging of IR pulse envelope and measurement of photoemission time delay.[5,26,27]

To better understand limitations of XPS with ultrashort pulses, it is important to consider the combined effects of the broadband pulse and the photoionization cross section. The photoionization cross section, particularly at energies well above the ionization threshold, exhibits weak dependence on the photon energy. In contrast, measurements conducted under resonant Raman conditions, where discrete levels in the continuum (such as autoionization or resonant states below the threshold) are encompassed by the broadband x-ray pulse, reveal distinct peaks in the electron spectra that provide insights into ultrafast dynamics.[28]

Resonant x-ray photoemission, also known as resonant Auger scattering (RAS), involves the excitation of a core-electron to an unoccupied molecular orbital, followed by the decay to a valence ionized state with the emission of an Auger electron. In the case of XPS with photon energy below the core-ionization threshold, the final state is similar to that of RAS, namely the valence ionized cation state. However, when the photon energy is tuned above the core-ionization threshold, XPS results in the emission of a core-electron. The spectra obtained in this process provide valuable information about the core-ionized states. Subsequently, decay occurs to the final double ionized state with the emission of a secondary Auger electron.

In this Letter, we provide a theoretical analysis of both types of XPS: below and above the core-ionization threshold of C 1*s* electron in the CO molecule. We compare these XPS spectra to the RAS spectra triggered by femtosecond and subfemtosecond x-ray pulses. Our results demonstrate that even in the case of attosecond pulses,

†These authors contributed equally to this work.
*Corresponding author. Email: song-bin.zhang@snnu.edu.cn
© 2023 Chinese Physical Society and IOP Publishing Ltd

RAS maintains high spectral resolution, unlike XPS. This finding highlights the potential applications of RAS utilizing ultrashort x-ray light sources. Unless otherwise stated, atomic units ($e = m_e = \hbar = 1$) are used throughout this study.

Figure 1 illustrates the scenarios of XPS and RAS processes triggered by non-resonant and resonant ultrashort x-ray pulses, respectively, using a showcase of the CO molecule. The RAS process involves the ground state $|\mathrm{G}\rangle$, intermediate core-excited state $|\mathrm{N}\rangle$, and final ionic state $|\mathrm{F}\rangle$, with corresponding potential energy curves (PECs) $V_\mathrm{G}(q)$, $V_\mathrm{N}(q)$, and $V_\mathrm{F}(q)$ (q is the internuclear distance). In the case of XPS, only the ground and final ionic states are involved. In the subsequent analysis, we simulate the XPS and RAS profiles while varying the x-ray pulse duration, ranging from several femtoseconds to sub-femtoseconds.

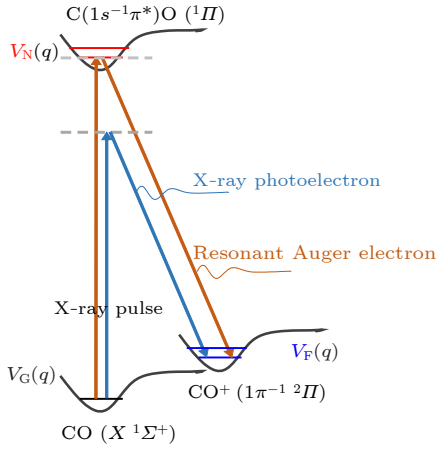

Fig. 1. Schematic illustration of the electronic states and PECs of the CO molecule coupled by non-resonant (XPS mode) and resonant (RAS mode) x-ray pulses. Both processes share the same initial and final states, while the RAS process also involves the intermediate core-excited state resonant to the pump pulse with the central frequency of $\omega = 287.4\,\mathrm{eV}$.

Our theoretical approach is based on a fully quantum time-dependent wave-packet technique, which has been comprehensively described in previous works.[29–38] The nuclear wave packet $\Psi_\gamma(t)$ is associated with the electronic state $|\gamma\rangle = |\mathrm{G}\rangle, |\mathrm{N}\rangle, |\mathrm{F}\rangle$, and ε is the energy of a released electron. Within the weak field approximation and under the rotating-wave and local approximations,[29,39–41] the total ε-dependent wave packet $\Psi(t) = [\Psi_\mathrm{G}(t), \Psi_\mathrm{N}(t), \Psi_\mathrm{F}(\varepsilon, t)]^\mathrm{T}$ for the RAS process can be expressed as[30,33,34]

$$i\dot{\Psi}(t) = \begin{pmatrix} V_\mathrm{G} & D^\dagger_\mathrm{GN}(t) & 0 \\ D_\mathrm{NG}(t) & V_\mathrm{N} - \omega - \dfrac{i\Gamma}{2} & 0 \\ D_\mathrm{FG}(t) & V_\mathrm{FN} & V_\mathrm{F} - \omega + \varepsilon \end{pmatrix} \Psi(t), \tag{1}$$

where $\Gamma = 2\pi \sum_\mathrm{F} |V_\mathrm{FN}|^2$ represents the total Auger decay width, which is determined by the Coulomb matrix element V_FN and the transition dipole interaction $D_\mathrm{NG}(t) = \frac{d_\mathrm{NG}}{2} g_0 g(t)$. The direct ionization channel $D_\mathrm{FG}(t) = \frac{d_\mathrm{FG}}{2} g_0 g(t)$ is negligible compared to the resonant excitation and is ignored in the RAS process. The seeded coherent XFEL is supposed,[21] which is characterized by a Gaussian envelope $g(t, \tau) = e^{-t^2/\tau^2}$ with electric field peak intensity g_0, pulse duration τ, and central frequency ω.

The Auger electron spectrum $\sigma(\varepsilon) = |\Psi_\mathrm{F}(\varepsilon, t \to \infty)|^2$ is computed as the norm squared of $\Psi_\mathrm{F}(\varepsilon, t)$ at long times, and it is typically expressed in terms of the binding energy $E_\mathrm{B} = \omega - \varepsilon$.[42] For modeling the XPS process, we omit the resonant channel (terms related to the core-excited state $|\mathrm{N}\rangle$) in the equation. The Auger width $\Gamma = 0.08\,\mathrm{eV}$, the PECs and transition dipole moments are taken from Refs. [33,43], and the molecular rotation is neglected during the ultrashort interaction time. Numerical simulations are performed using the multiconfiguration time-dependent Hartree method.[44,45]

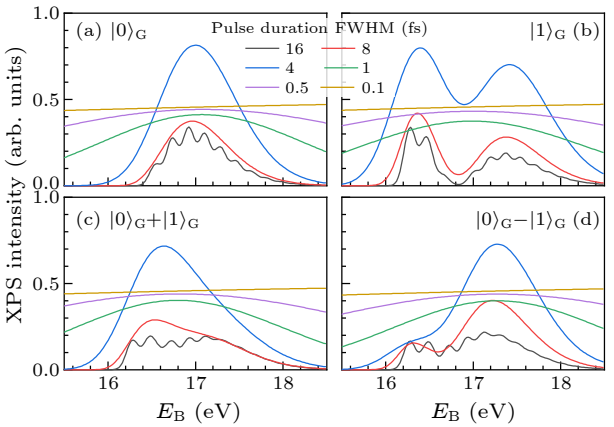

Fig. 2. XPS of CO molecule at the binding energy $E_\mathrm{B} = \omega - \varepsilon$ around 17 eV with excitation energy below the C 1s ionization threshold for x-ray pulse duration FWHM (full width at half maximum width) varied from 16 to 0.1 fs. Here ω and ε are the non-resonant pulse central frequency and photo electron energy, respectively. Panels (a) and (b) correspond to the XPS from the $\Psi_\mathrm{G}(t=0) = |0\rangle_\mathrm{G}$ and $|1\rangle_\mathrm{G}$ initial vibrational states, respectively; panels (c) and (d) show the XPS from superpositions of the two lowest vibrational levels, $\frac{1}{\sqrt{2}}(|0\rangle_\mathrm{G} + |1\rangle_\mathrm{G})$ and $\frac{1}{\sqrt{2}}(|0\rangle_\mathrm{G} - |1\rangle_\mathrm{G})$, respectively.

The XPS profiles obtained using a non-resonant x-ray pulse with varying pulse duration are shown in Fig. 2. We investigate the process starting from the lowest vibrational level ($\Psi_\mathrm{G}(t=0) = |0\rangle_\mathrm{G}$) and the first excited vibrational level ($|1\rangle_\mathrm{G}$) of the ground electronic state $|\mathrm{G}\rangle$. For a 16 fs pulse duration (full width at half maximum width, FWHM $= \sqrt{4 \ln 2}\tau$), the XPS profile [Fig. 2(a)] exhibits a well-resolved vibrational structure, resembling a conventional photoemission spectrum.[46] When initiated from the first excited vibrational state $|1\rangle_\mathrm{G}$, the XPS profile splits into two bands according to the reflection principle,[47] reflecting the nodal structure of the initial vibrational wave function. These bands are dressed by the vibrational structure of the final bound cation state. As the pulse duration decreases (e.g., the red curves corresponding to an 8 fs x-ray pulse), the vibrational structure in the XPS profile becomes smeared out. However, the nodal structure of the initial wave function can still be resolved up to a pulse duration of 1 fs [blue line in Fig. 2(b)]. With further reduction in pulse duration, even the nodal

structure becomes indistinguishable in the XPS profile.

At room temperature, the population of the lowest vibrational state is dominant in a molecule. However, by employing IR-pump spectroscopy, it is possible to create a coherent superposition of vibrational levels using an IR pulse.[47,48] In this scenario, the XPS spectra can probe the coherent superposition of the two vibrational levels $|0\rangle_{\rm G}$ and $|1\rangle_{\rm G}$. We consider that the vibrational levels are in-phase $\frac{1}{\sqrt{2}}(|0\rangle_{\rm G}+|1\rangle_{\rm G})$ and in anti-phase $\frac{1}{\sqrt{2}}(|0\rangle_{\rm G}-|1\rangle_{\rm G})$, as shown in Figs. 2(c) and 2(d), respectively. In both cases, the XPS spectra exhibit broad structures and show relatively small differences even for the longest x-ray pulse duration of 16 fs. Similar to the ionization from an individual vibrational level [Figs. 2(a) and 2(b)], reducing the pulse duration leads to a broadening of the spectra, eventually resulting in a structure-less and continuous profile at a pulse duration of FWHM = 0.1 fs.

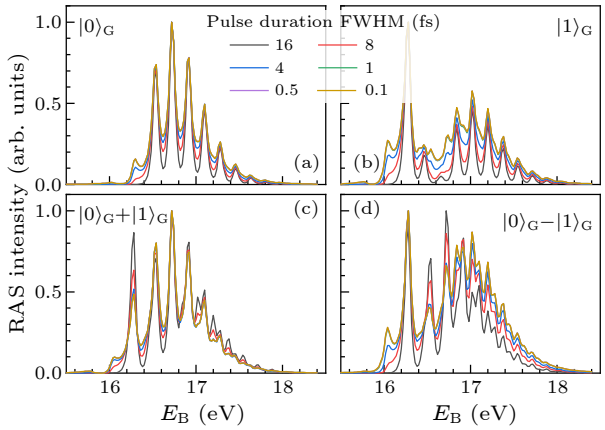

Fig. 3. RAS spectra with respect to the binding energy $E_{\rm B}=\omega-\varepsilon$ by resonant x-ray pulses with central frequency of $\omega=287.4$ eV. Here ε is the Auger electron energy. The description of panels is the same as in Fig. 2.

The situation is qualitatively different for the case of RAS, as shown in Fig. 3. In the conventional case of excitation from the lowest vibrational level, the RAS spectra closely resemble those obtained in synchrotron measurements,[49] where a narrow band excitation is used. However, in the case of RAS triggered by ultrashort pulses, which have a broad bandwidth, the contribution from several vibrational levels of the core-excited state becomes evident in the spectra. This can be observed in the development of lower binding energy shoulders in the spectra as the pulse duration decreases. Despite the presence of multiple vibrational levels, the overall resolution of the RAS spectra is not affected due to the resonant Raman condition.[28] When the excitation is from the second vibrational level, a two-band structure is formed in the spectra, following the reflection principle. This structure is dressed with the vibrational features of the final cation state, similar to what was discussed earlier for XPS. Notably, when the initial state is a superposition of the two lowest vibrational levels [Figs. 3(c) and 3(d)], the overall RAS spectra become sensitive to the duration of the x-ray pulse and exhibit different trends for the in-phase [Fig. 3(c)] and anti-phase [Fig. 3(d)] cases.

To gain a better understanding of the distinct and complementary characteristics of XPS and RAS in relation to pulse duration and initial state, we can conduct first- and second-order time-dependent perturbation analyses of Eq. (1) for XPS and RAS signals.[32,34,50] These analyses yield

$$\sigma^{\rm XPS}(E_{\rm B})=\sum_{\rm f}\Big|\sum_{\rm g}c_{\rm g}\frac{\sqrt{\pi}}{2}\tau\Omega_{\rm fg}e^{-\frac{\tau^2(E_{\rm fg}-E_{\rm B})^2}{4}}\Big|^2, \tag{2}$$

$$\sigma^{\rm RAS}(E_{\rm B})=\sum_{\rm f}\Big|\sum_{\rm n,g}c_{\rm g}\frac{\sqrt{\pi}}{2}\frac{\tau V_{\rm fn}\Omega_{\rm ng}e^{-\frac{\tau^2(E_{\rm fg}-E_{\rm B})^2}{4}}}{\omega-E_{\rm nf}-E_{\rm B}+\frac{i\Gamma}{2}}\Big|^2, \tag{3}$$

where $|{\rm g}\rangle$, $|{\rm n}\rangle$, and $|{\rm f}\rangle$ represent the vibrational levels of the electronic states $|{\rm G}\rangle$, $|{\rm N}\rangle$, and $|{\rm F}\rangle$, respectively. These states have corresponding total (electronic and vibrational) energies $E_{\rm g}$, $E_{\rm n}$, and $E_{\rm f}$. The energy differences between the states are denoted as $E_{\rm fg}=E_{\rm f}-E_{\rm g}$ and $E_{\rm nf}=E_{\rm n}-E_{\rm f}$. Here $c_{\rm g}$ represents the weight coefficient of the vibrational level $|{\rm g}\rangle$ in the total vibrational wave function of the ground state $\Psi_{\rm G}(t=0)=\sum_{\rm g}c_{\rm g}|{\rm g}\rangle$. The terms $V_{\rm fn}\simeq V_{\rm FN}\langle{\rm f}|{\rm n}\rangle$, $\Omega_{\rm fg}=\langle{\rm f}|\frac{d_{\rm FG}}{2}g_0|{\rm g}\rangle$, $\Omega_{\rm ng}=\langle{\rm n}|\frac{d_{\rm NG}}{2}g_0|{\rm g}\rangle$ and $\Omega_{\rm ng}=\langle{\rm n}|\frac{d_{\rm NG}}{2}g_0|{\rm g}\rangle$ correspond to the electronic-vibrational transition matrix elements between the $|{\rm ket}\rangle$ and $\langle{\rm bra}|$ states. These matrix elements are responsible for the coupling between the different vibrational levels and electronic states in the system.

As indicated by Eq. (2), the structure of $\sigma^{\rm XPS}(E_{\rm B})$ is influenced by both the transition matrix element $\Omega_{\rm fg}$ and the x-ray pulse spectrum in terms of $\exp[-\frac{\tau^2(E_{\rm fg}-E_{\rm B})^2}{4}]$. Since $\Omega_{\rm fg}$ is generally not sensitive to energy, the peaks of $\sigma^{\rm XPS}(E_{\rm B})$ are located near $E_{\rm B}=E_{\rm fg}$, with the peak intensity determined by the Franck–Condon factor $\sim\langle{\rm f}|{\rm g}\rangle^2$. The spectral structure can be significantly affected by the contributions from the initial vibrational levels $|{\rm g}\rangle$, represented by the coefficients $c_{\rm g}$. These observations are clearly evident in Fig. 2. In the case of a sub-femtosecond x-ray pulse with a bandwidth exceeding 3.0 eV, the structures originating from the initial and final states are smeared out, and the overall spectral structure of XPS is dominated by the broad x-ray pulse. As a result, the XPS spectrum becomes featureless when the pulse duration (FWHM) is shorter than 1 fs.

Let us now shift the focus to the RAS cross section given by Eq. (3), which exhibits a qualitatively different structure. In addition to contributions from the transition matrix element $\Omega_{\rm ng}$, pulse spectrum about $\exp[-\frac{\tau^2(E_{\rm fg}-E_{\rm B})^2}{4}]$, and Coulomb transition matrix element $V_{\rm fn}$, the structure of $\sigma^{\rm RAS}(E_{\rm B})$ is also influenced by a resonant denominator, which reflects the energy conservation law $E_{\rm B}=\omega-E_{\rm nf}$ with the broadening parameter Γ of the core-excited state. Since the x-ray frequency ω is approximately equal to $E_{\rm ng}$ in RAS, the peak position $E_{\rm fg}$ is near $\omega-E_{\rm ng}$, as dictated by the energy conservation law. In the case of narrow band excitation (when the bandwidth is smaller than Γ), the peak positions in the RAS spectrum are primarily determined by $E_{\rm fg}$ and the product of the Franck–Condon factors $\langle n|g\rangle^2$ and $\langle f|n\rangle^2$. This situation corresponds to experiments performed with synchrotron radiation or, in our case, to the longest pulse

duration of 16 fs [Fig. 3(a)], which is longer than the Auger lifetime (8.2 fs). It is well-known that, in the limit of monochromatic x-ray radiation, the resolution of RAS is mainly determined by the instrumental resolution of the spectrometer.[28,51,52]

With the pulse duration decreasing as shown in Fig. 3, the bandwidth of pulse spectrum gradually surpasses the Auger decay width. It does not affect the individual peak within the Auger width region, but arises broad background outside the Auger width region. However, the resonant energy conservation law in the denominator of RAS cross section, $1/(\omega - E_{\rm nf} - E_{\rm B} + \frac{i\Gamma}{2})$, restricts the peak position and broadening in the RAS spectrum. In the case of an attosecond pulse, where the pulse spectrum is essentially constant around $E_{\rm B} = E_{\rm fg}$, the spectral function can be factored out from the modulus square of Eq. (3). Consequently, the profile of $\sigma^{\rm RAS}(E_{\rm B})$ becomes independent of incoming x-ray pulse duration, as illustrated in Fig. 3. The effects of different initial states and their superposition are also clearly observed in RAS spectra generated by sub-femtosecond x-ray pulses, in contrast to the behavior observed in XPS.

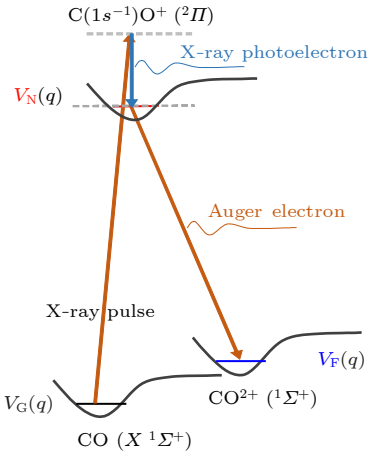

Fig. 4. Schematic of normal Auger decay of a CO molecule by x-ray pulse with central frequency above the K-absorption edge of the C atom, the photoelectron and Auger electron are released pertaining to the core-excited ionic state and dication state of CO, respectively.

Let us now examine XPS with ultrashort pulses having photon energy higher than the C 1*s* ionization threshold. In this case, as illustrated in Fig. 4, the spectra of photoemitted electrons correspond to the core-ionized state, in contrast to the valence ionization discussed in Fig. 2. It is important to note that the core-ionized state $C(1s^{-1})O^{+}(^{1}\Pi)$ subsequently decays to the double-cationic state $CO^{2+}(^{1}\Sigma^{+})$ with the emission of a secondary electron, whose spectrum is the focus of normal Auger electron spectroscopy (NAS).

In the normal Auger process, the photoelectron and Auger electron are coherently coupled, and coincidence measurements can identify both electrons from the same event due to their significantly different kinetic energies $\varepsilon_{\rm p}$ and $\varepsilon_{\rm a}$, respectively. Based on the theory for the normal Auger process with coherent x-ray pulses,[38] the total wave packet $\Psi(t) = [\Psi_{\rm G}(t), \Psi_{\rm N}(\varepsilon_{\rm p}, t), \Psi_{\rm F}(\varepsilon_{\rm p}, \varepsilon_{\rm a}, t)]^{\rm T}$ satisfies the time-dependent Schrödinger equation $i\dot{\Psi}(t) = H\Psi(t)$, where the Hamiltonian is given by

$$H = \begin{pmatrix} V_{\rm G} & 0 & 0 \\ D_{\rm NG}(t) & V_{\rm N} + \varepsilon_{\rm p} - \omega - \dfrac{i\Gamma}{2} & 0 \\ 0 & V_{\rm FN} & V_{\rm F} + \varepsilon_{\rm p} + \varepsilon_{\rm a} - \omega \end{pmatrix}. \tag{4}$$

Using the similar notation for the matrix elements and applying the perturbation theory, as performed above for RAS, we can express the photoelectron-Auger-electron-coincidence signal as

$$\sigma^{\rm pa}(\varepsilon_{\rm p}, \varepsilon_{\rm a}) = \sum_{\rm f} \left| \sum_{\rm n,g} c_{\rm g} \frac{\sqrt{\pi}}{2} \frac{\tau V_{\rm fn} \Omega_{\rm ng} e^{-\frac{\tau^2 (E_{\rm fg} + \varepsilon_{\rm p} + \varepsilon_{\rm a} - \omega)^2}{4}}}{\varepsilon_{\rm a} - E_{\rm nf} + \frac{i\Gamma}{2}} \right|^2. \tag{5}$$

As evident from Eq. (5), the structure of $\sigma^{\rm pa}(\varepsilon_{\rm p}, \varepsilon_{\rm a})$ is primarily determined by the pulse spectrum (exponential term) and the denominator term for energy conservation law $1/(\varepsilon_{\rm a} - E_{\rm nf} + \frac{i\Gamma}{2})$. This relationship is quite similar to that of RAS revealed in Eq. (3), allowing us to draw a similar conclusion that the coincidence signal $\sigma^{\rm pa}(\varepsilon_{\rm p}, \varepsilon_{\rm a})$ preserves sharp structures even in cases of using attosecond x-ray pulses.

The NAS signal $\sigma^{a}(\varepsilon_{\rm a})$ can be calculated from $\sigma^{\rm pa}(\varepsilon_{\rm p}, \varepsilon_{\rm a})$ by integrating over the photoelectron energy $\varepsilon_{\rm p}$. Since $\varepsilon_{\rm p}$ only appears in the exponential term of Eq. (5), the denominator term of Eq. (5) that determines the resolution of Auger spectra escapes the integration over $\varepsilon_{\rm p}$. As a result, $\sigma^{a}(\varepsilon_{\rm a})$ can also maintain energy resolution when using attosecond x-ray pulses.

On the other hand, for the XPS signal $\sigma^{p}(\varepsilon_{\rm p})$ of the core-ionized state, it can be evaluated by integrating the coincident signal $\sigma^{\rm pa}(\varepsilon_{\rm p}, \varepsilon_{\rm a})$ over the Auger energy $\varepsilon_{\rm a}$. However, such integration eliminates the denominator term in Eq. (5) and leaves only the exponential terms related to the pulse spectrum. This would undoubtedly smear out all the fine structures of XPS in the sub-femtosecond regime. These outcomes provide insights into the coincidence spectroscopy of normal Auger decay for HF molecules using ultrashort x-ray pulses.[38]

In conclusion, we have comprehensively investigated x-ray photoelectron spectroscopy (XPS) and resonant Auger electron spectroscopy (RAS) using ultrashort x-ray pulses, focusing on the CO molecule as a showcase. Additionally, normal Auger spectroscopy (NAS) for the photoelectron-Auger-electron-coincidence signal is also considered. The numerical calculations and analytical expressions presented in this work demonstrate that RAS and NAS can overcome the limitations of conventional XPS in terms of achieving high spectral resolution, for both valence and inner bands, when using attosecond x-ray pulses. Note that the present formulas of Auger signals involve more general cases with x-ray pulses, initial wavepacket and coherently coupled photoelectron and Auger electron, than the conventional Kramers–Heisenberg equation for monochromatic x-ray.[28] The application of (resonant) Auger electron spectroscopy with attosecond x-ray pulses provides valuable complementary information to photoelectron spectra, enabling the tracking of electronic and

molecular dynamics. These findings may highlight the promising potential of attosecond x-ray pulses in spectroscopy and related fields.

Acknowledgments. This work was supported by the National Natural Science Foundation of China (Grant Nos. 11934004 and 11974230), and Russian Science Foundation (Grant No. 21-12-00193).

References

[1] Turner D W 1970 *Philos. Trans. R. Soc. London. Ser. A* **268** 7
[2] Chastain J and King J R C 1992 *Handbook of X-Ray Photoelectron Spectroscopy* (Perkin-Elmer Corporation)
[3] Hüfner S 2013 *Photoelectron Spectroscopy: Principles and Applications* (Berlin: Springer)
[4] Lewenstein M, Balcou P, Ivanov M Y, L'Huillier A, and Corkum P B 1994 *Phys. Rev. A* **49** 2117
[5] Paul P M, Toma E S, Breger P, Mullot G, Augé F, Balcou P, Muller H G, and Agostini P 2001 *Science* **292** 1689
[6] McNeil B W J and Thompson N R 2010 *Nat. Photon.* **4** 814
[7] Amann J, Berg W, Blank V *et al.* 2012 *Nat. Photon.* **6** 693
[8] Allaria E, Appio R, Badano L *et al.* 2012 *Nat. Photon.* **6** 699
[9] Inhester L, Li Z, Zhu X *et al.* 2019 *J. Phys. Chem. Lett.* **10** 6536
[10] Pathak S, Ibele L M, Boll R *et al.* 2020 *Nat. Chem.* **12** 795
[11] LaForge A C, Michiels R, Ovcharenko Y *et al.* 2021 *Phys. Rev. X* **11** 021011
[12] Blanchet V, Zgierski M Z, Seideman T, and Stolow A 1999 *Nature* **401** 52
[13] Zewail A H 2000 *J. Phys. Chem. A* **104** 5660
[14] Neumark D M 2001 *Annu. Rev. Phys. Chem.* **52** 255
[15] Stolow A, Bragg A E, and Neumark D M 2004 *Annu. Rev. Phys. Chem.* **104** 1719
[16] Wu G R, Hockett P, and Stolow A 2011 *Phys. Chem. Chem. Phys.* **13** 18447
[17] Sansone G, Benedetti E, Calegari F *et al.* 2006 *Science* **314** 443
[18] Chini M, Zhao K, and Chang Z 2014 *Nat. Photon.* **8** 178
[19] Hartmann N, Hartmann G, Heider R *et al.* 2018 *Nat. Photon.* **12** 215
[20] Duris J, Li S, Driver T *et al.* 2020 *Nat. Photon.* **14** 30
[21] Maroju P K, Grazioli C, Fraia M D *et al.* 2020 *Nature* **578** 386
[22] Kaldun A, Blättermann A, Stooß V *et al.* 2016 *Science* **354** 738
[23] Kobayashi Y, Chang K F, Zeng T, Neumark D M, and Leone S R 2019 *Science* **365** 79
[24] Peng L Y, Jiang W C, Geng J W, Xiong W H, and Gong Q 2015 *Phys. Rep.* **575** 1
[25] Wang C, Gong M, Cheng Y *et al.* 2023 *J. Phys. Chem. Lett.* **14** 5475
[26] Itatani J, Quéré F, Yudin G L, Ivanov M Y, Krausz F, and Corkum P B 2002 *Phys. Rev. Lett.* **88** 173903
[27] Goulielmakis E, Yakovlev V S, Cavalieri A L *et al.* 2007 *Science* **317** 769
[28] Gel'mukhanov F, Odelius M, Polyutov S P, Föhlisch A, and Kimberg V 2021 *Rev. Mod. Phys.* **93** 035001
[29] Pahl E, Meyer H D, and Cederbaum L 1996 *Z. Phys. D: At. Mol. Clusters* **38** 215
[30] Demekhin P V, Chiang Y C, and Cederbaum L S 2011 *Phys. Rev. A* **84** 033417
[31] Zhang S B and Rohringer N 2014 *Phys. Rev. A* **89** 013407
[32] Zhang S B and Rohringer N 2015 *Phys. Rev. A* **92** 043420
[33] Zhang S B, Kimberg V, and Rohringer N 2016 *Phys. Rev. A* **94** 063413
[34] Zhang S B, Xie X T, and Wang J G 2017 *Phys. Rev. A* **96** 053420
[35] Bian Q, Wu Y, Wang J G, and Zhang S B 2019 *Phys. Rev. A* **99** 033404
[36] Shi X, Wu Y, Wang J G, Kimberg V, and Zhang S B 2020 *Phys. Rev. A* **101** 023401
[37] Zhu Y P, Liu Y R, Zhao X, Kimberg V, and Zhang S B 2021 *Chin. Phys. Lett.* **38** 053201
[38] Zhu Y P, Zhao X, Liu X J, Kimberg V, and Zhang S B 2022 *Phys. Rev. A* **106** 023105
[39] Demekhin P V and Cederbaum L S 2011 *Phys. Rev. A* **83** 023422
[40] Cederbaum L S and Domcke W 1981 *J. Phys. B* **14** 4665
[41] Domcke W 1991 *Phys. Rep.* **208** 97
[42] Kukk E, Bozek J D, Cheng W T, Fink R F, Wills A A, and Berrah N 1999 *J. Chem. Phys.* **111** 9642
[43] Skytt P, Glans P, Gunnelin K *et al.* 1997 *Phys. Rev. A* **55** 134
[44] Beck M H, Jäckle A, Worth G A, and Meyer H D 2000 *Phys. Rep.* **324** 1
[45] Worth G A, Beck M H, Jäckle A, Vendrell O and Meyer H D 2000 *The MCTDH Package*, Version 8.2. Meyer H D, Version 8.3 (2002), Version 8.4 (2007). Vendrell O and Meyer H D Version 8.5 (2013). Version 8.5 contains the ML-MCTDH algorithm. Current versions: 8.4.18 and 8.5.11 (2019). Used version: exchange with "Used version". See http://mctdh.uni-hd.de/
[46] Osborne S J, Ausmees A, Svensson S, Kivimäki A, Sairanen O P, de Brito A N, Aksela H, and Aksela S 1995 *J. Chem. Phys.* **102** 7317
[47] Ignatova N, da Cruz V V, Couto R C, Ertan E, Odelius M,Ågren H, Guimarães F F, Zimin A, Polyutov S P, Gel'mukhanov F, and Kimberg V 2017 *Phys. Rev. A* **95** 042502
[48] Liu J C, Savchenko V, Kimberg V, Odelius M, and Gel'mukhanov F 2021 *Phys. Rev. A* **103** 022829
[49] Carravetta V, Gel'mukhanov F K, Ågren H, Sundin S, Osborne S J, de Naves B A, Björneholm O, Ausmees A, and Svensson S 1997 *Phys. Rev. A* **56** 4665
[50] Shankar R 2012 *Principles of Quantum Mechanics* (Berlin: Springer Science & Business Media)
[51] Gel'Mukhanov F K, Mazalov L N, and Kondratenko A V 1977 *Chem. Phys. Lett.* **46** 133
[52] Correia N, Flores-Riveros A, Ågren H, Helenelund K, Asplund L, and Gelius U 1985 *J. Chem. Phys.* **83** 2035